Brain, Behavior, and Immunity 50 (2015) 87–100

Contents lists available at ScienceDirect

Brain, Behavior, and Immunity

journal homepage: www.elsevier.com/locate/ybrbi

Extracellular ATP enhances radiation-induced brain injury through microglial activation and paracrine signaling via P2X7 receptor

Pengfei Xu [a,b,1], Yongteng Xu [a,b,1], Bin Hu [a], Jue Wang [a], Rui Pan [a], Madhuvika Murugan [c], Long-Jun Wu [c], Yamei Tang [a,b,*]

[a] Department of Neurology, Sun Yat-Sen Memorial Hospital, Sun Yat-Sen University, Guangzhou 510120, China
[b] Guangdong Provincial Key Laboratory of Malignant Tumor Epigenetics and Gene Regulation, Sun Yat-Sen Memorial Hospital, Sun Yat-Sen University, Guangzhou 510120, China
[c] Department of Cell Biology and Neuroscience, Rutgers University, Piscataway, NJ 08854, United States

ARTICLE INFO

Article history:
Received 2 April 2015
Received in revised form 24 June 2015
Accepted 24 June 2015
Available online 27 June 2015

Keywords:
Extracellular ATP
P2X7R
Microglia
Radiation-induced brain injury
Inflammation
COX-2
TNF-α
IL-6
BBG

ABSTRACT

Activation of purinergic receptors by extracellular ATP (eATP) released from injured cells has been implicated in the pathogenesis of many neuronal disorders. The P2X7 receptor (P2X7R), an ion-selective purinergic receptor, is associated with microglial activation and paracrine signaling. However, whether ATP and P2X7R are involved in radiation-induced brain injury (RBI) remains to be determined. Here, we found that the eATP level was elevated in the cerebrospinal fluid (CSF) of RBI patients and was associated with the clinical severity of the disorder. In our experimental model, radiation treatment increased the level of eATP in the supernatant of primary cultures of neurons and glial cells and in the CSF of irradiated mice. In addition, ATP administration activated microglia, induced the release of the inflammatory mediators such as cyclooxygenase-2, tumor necrosis factor α and interleukin 6, and promoted neuronal apoptosis. Furthermore, blockade of ATP–P2X7R interaction using P2X7 antagonist Brilliant Blue G or P2X7 knockdown suppressed radiation-induced microglial activation and proliferation in the hippocampus, and restored the spatial memory of irradiated mice. Finally, we found that the PI3K/AKT and nuclear factor κB mediated pathways were downstream of ATP–P2X7R signaling in RBI. Taken together, our results unveiled the critical role of ATP–P2X7R in brain damage in RBI, suggesting that inhibition of ATP–P2X7R axis might be a potential strategy for the treatment of patients with RBI.

1. Introduction

Radiotherapy is the mainstay of therapy for head and neck cancers, and its curative efficacy is well-established. However, radiotherapy can also cause injury to the adjacent normal brain tissue and lead to neurological complications (Dietrich et al., 2008; Wang et al., 2010). Radiation-induced brain injury (RBI) is common and severely influences the quality of life of patients. Aside from the use of steroids (Genc et al., 2006) or bevacizumab (Matuschek et al., 2011), which provide protection to a subset of patients, no other effective treatments for RBI are currently available. Moreover, steroids have severe side effects (Noone, 2006), with reports showing exacerbation of cerebral radiation necrosis in certain patients treated with bevacizumab (Jeyaretna et al., 2011). Therefore, a comprehensive investigation of RBI pathogenesis is required to identify novel therapeutic targets and develop a better treatment and prevention for RBI.

In the adult brain, resting microglia are activated and transformed from a ramified to an amoeboid morphology in response to injury (Prinz and Priller, 2014). Activated microglia release various proinflammatory mediators, such as cyclooxygenase-2 (COX-2), tumor necrosis factor α (TNF-α), and interleukin 6 (IL-6) (Choi et al., 2011; Gonzalez-Scarano and Baltuch, 1999), leading to neuronal injury, impairment of tissue repair and neuronal degeneration (Hu et al., 2014). Consistently, the release of proinflammatory mediators by activated microglia plays a pivotal role in the underlying pathology of RBI (Chen and Palmer, 2013; Monje et al., 2003; Yoritsune et al., 2014). However, the trigger for microglial release of proinflammatory mediators in RBI remains to be elucidated.

Abbreviations: eATP, extracellular ATP; BBG, Brilliant Blue G; P2X7R, P2X7 receptor; GVHD, graft-versus-host disease; RBI, radiation-induced brain injury; TNF, tumor necrosis factor; oxATP, oxidized ATP; CSF, cerebrospinal fluid.

* Corresponding author at: Department of Neurology, Sun Yat-Sen Memorial Hospital, Sun Yat-Sen University, No. 107, Yan Jiang Xi Road, Guangzhou, Guangdong Province 510120, China.
E-mail address: yameitang@hotmail.com (Y. Tang).
[1] These authors contributed equally to the study.

http://dx.doi.org/10.1016/j.bbi.2015.06.020
0889-1591/

Excessive release of eATP following tissue injury can activate microglia and is implicated in pathological conditions such as spinal cord and ischemia reperfusion injuries (Cheng et al., 2014; Fields and Stevens, 2000; Kobayashi et al., 2013). Among the ATP-sensitive purinergic receptors, the P2X7 receptor (P2X7R) is expressed abundantly in the central nervous system (CNS) (Lister et al., 2007), particularly in microglia. The upregulation of P2X7R expression in activated microglia has been reported in many neuropathological conditions, including amyotrophic lateral sclerosis (Gandelman et al., 2010), kainate-induced seizures (Engel et al., 2012), neuropathic pain (Makoto et al., 2012).

The role of ATP-mediated signaling in RBI remains largely unknown. Specifically, it is still unknown whether ATP concentration alters after radiation and if this change could activate microglial P2X7R to amplify the inflammatory response and subsequently result in brain injury. Here we found a positive correlation between the ATP levels and severity of RBI. To further our understanding, we investigated the role of P2X7R in ATP-mediated inflammatory responses to brain injury using an *in vivo* and *in vitro* irradiation model based on previous studies (Hwang et al., 2006; Peng et al., 2014). The results of this study, suggests that ATP–P2X7R signaling plays a critical role in the pathogenesis of RBI and its inhibition might be a potential strategy to ameliorate radiation-induced neuronal damage in patients with RBI.

2. Materials and methods

2.1. Ethics statement

This study was approved by the Human Research Review Board of Sun Yat-Sen Memorial Hospital and was performed in accordance with the Declaration of Helsinki. Written informed consent was obtained from all participants. BALB/c mice (male) were obtained from the Laboratory Animal Center of Sun-Yet Sen University. All animal procedures followed the humane care guidelines of the Chinese National Institute of Health, and the protocols were approved by the Committee on Animal Research of Sun Yat-Sen University.

2.2. Participants

A total of 36 patients (10 females and 26 males) from Sun Yat-Sen Memorial Hospital who were diagnosed as having RBI after radiotherapy for nasopharyngeal carcinoma were enrolled between October 2010 and March 2012. Radiographic evidence to support the diagnosis of RBI without tumor recurrence or metastases was available for all subjects. The diagnosis of RBI was defined as a lesion of high intensity on T2-weighted images and as a lesion of enhancement on post-contrast images, as described in our previous study (Tang et al., 2014). The control group (8 females and 47 males) included ten patients without RBI after radiotherapy for nasopharyngeal carcinoma and 45 individuals who underwent check-up but had no CNS diseases. The subjects in the control group did not show lesions on magnetic resonance imaging (MRI) scans. The detailed patient characteristics are listed in Supplementary Table 1. CSF samples were collected from both case and control group. Control participants were those with complains of limb numbness, dizziness or similar symptoms, but diagnosed to be devoid of CNS disorders.

2.3. Evaluation of neurological symptoms and edema volumes on MRI scans

The pre-treatment medical histories and results of physical examinations of the subjects were evaluated. Neurological signs and symptoms were assessed using the Late Effects in Normal Tissues, Subjective, Objective, Management, Analytic (LENT-SOMA) scales (Routledge et al., 2003). The MRI evaluation of radiation injury included measurements of the edema volume on T2-weighted Fluid-Attenuated Inversion Recovery (FLAIR) images and the necrotic volume on gadolinium-enhanced areas of T1-weighted images. The radiologist used manual and semiautomatic approaches to identify the outline of the edema, and then the total edema volume was estimated using Volume Viewer 2 software (GE, AW Suite 2.0 6.5.1.z). To determine the necrotic volume, the radiologist defined the gadolinium-enhanced area to identify the outline of the lesion, and then the area was calculated automatically using Volume Viewer 2. Because the intracranial volume differs between patients, the edema and necrotic volumes were normalized using the mid-sagittal cross-sectional intracranial area, a surrogate measurement of the intracranial volume (Ferguson et al., 2005; Nandigam et al., 2007). All MRI studies were evaluated by a radiologist who was blinded to the grouping.

2.4. Reagents

The culture medium materials (Dulbecco's Modified Eagle Medium-F12, B-27 supplement, and fetal bovine serum) were purchased from GIBCO (USA). Trypsin–EDTA, DNase I, L-glutamine, and gentamycin were purchased from Sigma (USA). Brilliant Blue G (BBG) and ATP were purchased from Sigma (USA). The following antibodies were used: rat anti-CD11b (AbD Serotec, UK), rabbit anti-IBA1 (Wako, Japan), rabbit anti-COX2 (Millipore, USA), mouse anti-NeuN (Millipore, USA), rabbit anti-tubulin (Millipore, USA), and rabbit anti-P2X7R (Alomone Labs, Israel). The fluorescent secondary antibodies labeled with FITC, Alexa-488, Alexa-594 and Cy3 were purchased from Jackson ImmunoResearch Laboratories (USA). The Fluorescein FragEL DNA Fragmentation Detection (TUNEL) Kit was purchased from Millipore (USA). The RT-PCR and quantitative PCR kits were purchased from TaKaRa (Japan). Enzyme-linked immunoabsorbent assay (ELISA) kits to measure TNF-α, COX-2, and IL-6 were obtained from Dakewei (China). The ATPlite 1step kit was purchased from PerkinElmer (Waltham, USA). The Western blotting reagents and secondary antibodies were purchased from WeiJia Inc. (China), and the PVDF membrane was purchased from Millipore (USA). Experimental equipment was supplied by Sun Yat-Sen Memorial Hospital of Sun Yat-Sen University.

2.5. Cell culture and irradiation

Primary microglia derived from newborn mice were prepared from mixed glial cultures using the "shaking off" method, as described previously (Suzumura et al., 1987). Briefly, pups were sterilized with 70% ethanol, the brain tissue was placed on ice cold HBSS. The meninges, cerebellum and brain stem were removed under a dissection microscope. The remaining tissue was chopped into small pieces, washed with serum-free DMEM and then digested with a mix of papain (30 U/ml), Dnase I (200 μg/ml), EDTA (0.5 mM) and L-cysteine (0.2 mg/ml) for 30 min at 37 °C. The mixture was then spun down; the pellet was carefully suspended in DMEM with 10% fetal bovine serum and cells transferred into a T75 flask. After 24 h the medium (DMEM supplemented with 10% fetal bovine serum, 1 mM Na + pyruvate, 100 units/ml penicillin, and 100 μg/ml streptomycin) was changed. The cells were cultured until rounded, shiny microglial cells started to float off the astrocyte layer. These cells were shaken off, collected, washed with DMEM for further experiments. The primary cultured neurons and astrocytes were harvested from the hippocampi of postnatal day 0 embryonic mice, as reported previously (Wang et al., 2011). The cells were randomly divided into four groups: control,

radiation, ATP, radiation with ATP pre-treatment, and radiation with BBG pre-treatment. Where relevant, the cells were pre-incubated with BBG (1 μM final concentration) or ATP (10 μM or 100 μM final concentration) for 1 h before radiation. The concentrations and pre-treatment times were determined in previous experiments. The cells were irradiated with 10 Gy at a dose rate of 6 MeV/min using a linear accelerator (Siemens, German), and then returned to the incubator and maintained at 37 °C and 5% CO_2. The cultured cells were prepared for PCR, Western blotting, and immunofluorescence analyses. The regimen of cell irradiation was based on our previous study. We tested the radiation dose effect from 3, 5, 8 to 10 Gy. We found that inflammatory mediators did not change at 3 or 5 Gy, but increased significantly at 8 and 10 Gy. Referring to study that indicated 10 Gy was the optimal dosage to activate microglia (Hwang et al., 2006), we applied 10 Gy in the cell irradiation.

2.6. Animals and irradiation

Adult male mice ($n = 65$; weight, 18–22 g) were randomly divided into the following groups: non-irradiated controls, irradiated mice, and irradiated mice administered BBG. Mice in the final group received an intraperitoneal injection of BBG (50 mg/kg/day) 2 h before irradiation, for 7 consecutive days. Mice in the control and irradiation alone groups were injected with the same volume of saline. Animal irradiation was performed using a 6 MV β-ionizing-ray linear accelerator (Siemens, Germany). The head of each mouse was placed in a treatment field (2×2 cm^2) within the confines of the whole-brain from the post-canthus line to the post-aurem line. A single dose of 30 Gy was given at a dose rate of 3 Gy/min and a source-to-skin distance of 100 cm. In previous study, single dose higher than 25 Gy were applied to induce brain injury in rats (Panagiotakos et al., 2007). Study showed that microglial-derived COX-2 did not increase if the dose was less than 25 Gy (Olschowka et al., 1997). We therefore used a single dose of 30 Gy for *in vivo* irradiation. The animals were sacrificed 3, 7, and 14 days after irradiation, or were followed for 8 weeks to evaluate their spatial learning activities. These time points were decided according to our previous study, showing that the gene and protein expression alteration occurs as early as 3 days, morphological change 7 days, while cognition impairment 8 weeks (Peng et al., 2014). For detection of neurogenesis in the dentate gyrus, bromodeoxyuridine (BrdU) (Sigma, USA) at 100 mg/kg i.p. was administered started 7 days before sacrificed, once daily for 6 consecutive days, and then three times on the day of sacrifice (10 h, 6 h and 2 h prior to sacrifice).

2.7. Collection of cerebrospinal fluid from the mouse cisterna magna

Cerebrospinal fluid (CSF) was collected from the mouse cisterna magna using Liu's procedure (Liu and Duff, 2008). Briefly, after the mice were deeply anesthetized, the necks were shaved and the mice were placed on the stereotaxic instrument. The surgical equipment was sterilized thrice using 10% povidone iodine and 70% ethanol. The animal's head was placed at an angle of approximately 135° to the body. A sagittal incision was made inferior to the occiput, and the subcutaneous tissue and muscles were separated until the medulla oblongata and CSF space were visible. A capillary tube was placed into the cisterna magna, and CSF was collected in a capillary tube. The mice were sutured and placed in a 37 °C incubator for recovery.

2.8. Inhibiting P2X7R expression using short interfering RNAs

Primary microglia in 6-well plates were maintained in proliferating medium for 2 days. Cells at 30–50% confluence were transfected with a negative control short interfering RNA (siRNA) (5′-UUCUCCGAACGUGUCACGUTT-3′) or a P2X7R-specific siRNA (5′-CCGUACUCAUCAAGAAUAATT-3′), both of which were synthesized by GenePharma (Shanghai, China). Briefly, to prepare the transfection mixture, Transfectamine (5 μl; Invitrogen) and siRNA (10 μl) were added individually to Opti-MEM® Reduced Serum Medium (final volume of 250 μl) and incubated for 5 min. The siRNA and Transfectamine solutions were then combined, mixed by gentle pipetting, and incubated at room temperature for 20 min. Prior to the addition of the transfection mixture, the cells were washed with Opti-MEM, and then a 1500 μl aliquot of fresh Opti-MEM was added to each well. The transfection mixture was added to the cells in a drop-wise manner, and the cells were incubated at 37 °C for 20 min. Primary microglia were treated with the negative control or P2X7R-specific siRNA for 6 h. Gene and protein expression levels were detected by real-time PCR and Western blot analysis, respectively.

2.9. Quantitative PCR and RT-PCR

Total RNA was isolated from cells using the RNeasy Plus Mini Kit (TaKaRa), according to the manufacturer's instructions. After reverse transcription, quantitative real-time PCR was performed using primers specific for the genes encoding P2X7R and inflammatory mediators IL-6, COX-2, and TNF-α. Fast thermal cycling was performed using a Real-Time PCR System (Roche LightCycler 480) under the following conditions: denaturation at 95 °C for 10 s, followed by 40 cycles of 95 °C for 10 s, 60 °C for 10 s, and 72 °C for 20 s. Semi-quantitative PCR experiments were also performed using primers that specifically amplified the C-terminal region of the full-length transcript encoding the P2X7R. The results were expressed as the relative mRNA expression of the threshold cycle value, and were normalized by parallel amplification of the endogenous control GAPDH. The target mRNA expression level in control group (target mRNA/GAPDH value) was set to 100%, and the mRNA in other groups were converted to fold changes after comparing to the control group.

2.10. Western blotting

Total protein (20 μg) was electrophoresed through a 10% SDS–PAGE gel and transferred to a PVDF membrane. Western blotting was performed with the following primary antibodies: polyclonal rabbit anti-P2X7R (1:350), monoclonal rabbit anti-COX-2 (1:200), and anti-GAPDH (1:500). The filters were incubated with the primary antibody in 5% dried non-fat milk at 4 °C overnight. A secondary goat anti-rabbit polyclonal antibody (1:500) was used prior to chemiluminescent detection. An imaging densitometer scanner controlled by the Quantity One PC software (Bio-Rad, USA) was used to detect the signals. In all cases, the average intensity of the pixels in a background-selected region was calculated and subtracted from each pixel in the sample. To correct for deviation, the densitometry values obtained in the linear range of detection were normalized to those obtained for GAPDH. Statistical analysis was performed using a one-way ANOVA, followed by the Bonferroni correction.

2.11. Immunohistochemistry and immunocytochemistry

After being anesthetized with 10% chloral hydrate (4 ml/kg), the animals received were perfused with phosphate-buffered saline (PBS) and then 4% paraformaldehyde. After perfusion, the brains were removed quickly and post-fixed in 4% paraformaldehyde overnight. The brains were then dehydrated in a gradient sucrose solution (10%, 20%, and 30%) at 4 °C. Serial sections of mouse brains (10 μm thickness) were cut using a cryostat. The microscope slides

containing the brain slices were stored temporarily in cryoprotectant solution at 30 °C until morphological staining. After rinsing with 0.3% Triton X-100 for 30 min at 37 °C, the sections were blocked in solution containing 5% normal goat serum for 1 h, and then washed several times. The sections were then incubated with the following primary antibodies at 4 °C overnight: polyclonal anti-IBA1 (1:400, for microglia of brain section), monoclonal anti-NeuN (1:300), monoclonal anti-tubulin (1:1000), and polyclonal rabbit anti-P2X7R (1:200). The primary antibodies were detected by incubation of the sections with Alexa-488- and Alexa-594-conjugated secondary antibodies (1:500) at room temperature for 1 h. The sections were cover-slipped with glycerol and detected using an Olympus BX5 microscope. The percentage of activated microglial cells was determined for each group. For each repeated experiment, the numbers of $IBA1^+$ cells were counted in six random fields (200× magnification). Resting microglia exhibited a branch-like form, while activated microglial cells were characterized by bigger soma and round or amoeboid shapes.

For immunocytochemistry, the cells were washed twice with PBS, fixed with 4% paraformaldehyde for 20 min, and then blocked with 5% goat serum albumin for 1 h. The cells were then incubated with a monoclonal rat anti-CD11b antibody (1:100, for cultured primary microglia) at 4 °C overnight, washed three times with PBS, incubated with rat anti-rabbit Cy3-conjugated secondary antibodies (1:500) for 1 h in a 37 °C thermostat incubator, and then cover-slipped with anti-fluorescence-quenching reagent (Boshide, China). After DAPI staining, the fluorescent images were detected and analyzed as described above. Resting microglia had relatively small soma with thin protrusions, while activated microglia had amoeboid shapes with bigger soma and thicker but shorter protrusions. For each repeated experiment, the cells were counted in six random fields (200× magnification).

After incubation of cultured neurons with 100 nM ATP for 24 h, the cells were double stained using a NeuN and TUNEL kit, according to the manufacturer's instructions. The fluorescent imaging was performed and analyzed as described above.

2.12. ELISA

Primary microglia, astrocytes, and neurons (2×10^6 in 2 ml of medium) were seeded into 60 mm dishes and treated as indicated. The radiation plus BBG or ATP groups were pre-treated with BBG or ATP for 60 min. The radiation and radiation plus BBG or ATP groups were exposed to 10 Gy radiation. The supernatants were collected 24 h and 48 h after irradiation and analyzed using an ATP Fluorometric Assay Kit (BioVision, Cat. No. K354–100), according to the manufacturer's instructions. All samples were stored at −80 °C until the ELISAs. The standard samples and control groups were added to the corresponding wells. The biotin-labeled primary antibody (diluted to 1 μg/ml in blocking buffer) was added to each well (50 μl/well), and the plate was incubated with agitation at 37 °C for 90 min. The plate was then washed four times with washing buffer, and a secondary HRP-conjugated antibody (diluted in blocking buffer according to the manufacturer's instructions) was added to each well (100 μl/well). Subsequently, the plate was washed five times with wash buffer. TMB substrate (100 μl) was added to each well, and the plate was incubated in the dark at room temperature for 30 min. Finally, the reaction was stopped by the addition of stop solution (100 μl/well). The absorbance at 595 nm was determined using a microplate reader, and the data were analyzed using SoftMax Pro Software.

The ATP levels in CSF samples of participants were measured using ATPlite 1step kit (PerkinElmer) according to the guideline protocol. The emitted light, produced by the reaction of ATP with added luciferase and D-luciferin, is proportional to the concentration of ATP. In a 96-well black clear-bottom plate, 100 μL of the reconstituted reagent were added to each well containing 2×10^4 -cells (100 μL), equilibrated at room temperature. The plate was shaken for 2 min at 700 rpm using an orbital microplate shaker, then the luminescence was measured using a multiwell plate reader (Wallac Victor2, PerkinElmer).

2.13. Morris water maze

Spatial learning and memory were evaluated at 8 weeks post-irradiation using the Morris water maze, as described previously (Peng et al., 2014). Mice were trained in the Morris water maze for 7 days with four trials per day ($n = 6$ animals per group). The latency in finding the platform and the swim path length were analyzed using a computerized video tracking system (DMS-2). The probe trial was performed on day 7, during which the mice were allowed to explore the water maze platform with the platform removed for 60 s. The time spent in each quadrant and platform location crossings were recorded for the 60 s probe trial. After the maze test, the animal was dried with a towel and returned to its cage located next to an electric radiator.

2.14. Statistics

All experiments were repeated at least three times, and the results are presented as the mean ± SEM. The statistical significance of the differences was analyzed using Student's *t*-test between two groups and One-way ANOVA with Bonferroni's correction for multiple group comparison. For analysis of Morris water Maze, ANOVA with repeated measures (compound by exercise by days) was used for path length and latency. One-way ANOVA was applied to analyze the probe trials. Pearson's correlation coefficient was used for correlation analyses, $R > 0.8$ reflected a high positive correlation, $0.3 < R < 0.8$ reflected a moderate positive correlation, and $R < 0.3$ reflected no correlation. $P < 0.05$ was considered statistically significant.

3. Results

3.1. The ATP level in the CSF is positively correlated with the severity of RBI

The release of ATP from injured cells can trigger cellular injury (Haag et al., 2007), indicating a possible relationship between eATP and neuronal damage in RBI. To test this hypothesis, the ATP levels in CSF samples from patients with (case group) and without (control group) RBI were compared. We found that the levels of eATP in CSF of case group were higher than those of control group (Fig. 1A). There was a positive correlation between the concentration of eATP and the SOMA score ($R = 0.883$, $P < 0.001$), the brain edema volume ($R = 0.906$, $P < 0.001$), and the necrosis volume ($R = 0.738$, $P < 0.001$), suggesting that elevated levels of eATP are associated with aggravated symptoms of RBI (Fig. 1B). Moreover, the levels of inflammatory mediators (COX-2, IL-6, and TNF-α) were also increased in the case group than in the control group (Fig. 1C), and these upregulated levels were positively correlated with the elevated eATP levels (Fig. 1D; $R_{COX\text{-}2} = 0.938$, $R_{IL\text{-}6} = 0.845$, $R_{TNF\text{-}a} = 0.902$ and all $P < 0.001$).

Next, we used a mouse model of RBI in which mice undergoing whole brain irradiation with a single dose of 30 Gy and measured the levels of eATP in the CSF of RBI mice. At 3 and 7 days post-irradiation, the eATP levels in the CSF of the irradiated mice were significantly higher than those in the control mice (Fig. 1E). To further confirm that ATP is released by irradiation-induced cell damage, we exposed primary microglia, astrocytes, and neurons to a single 10 Gy dose of radiation. Consistently, we found an

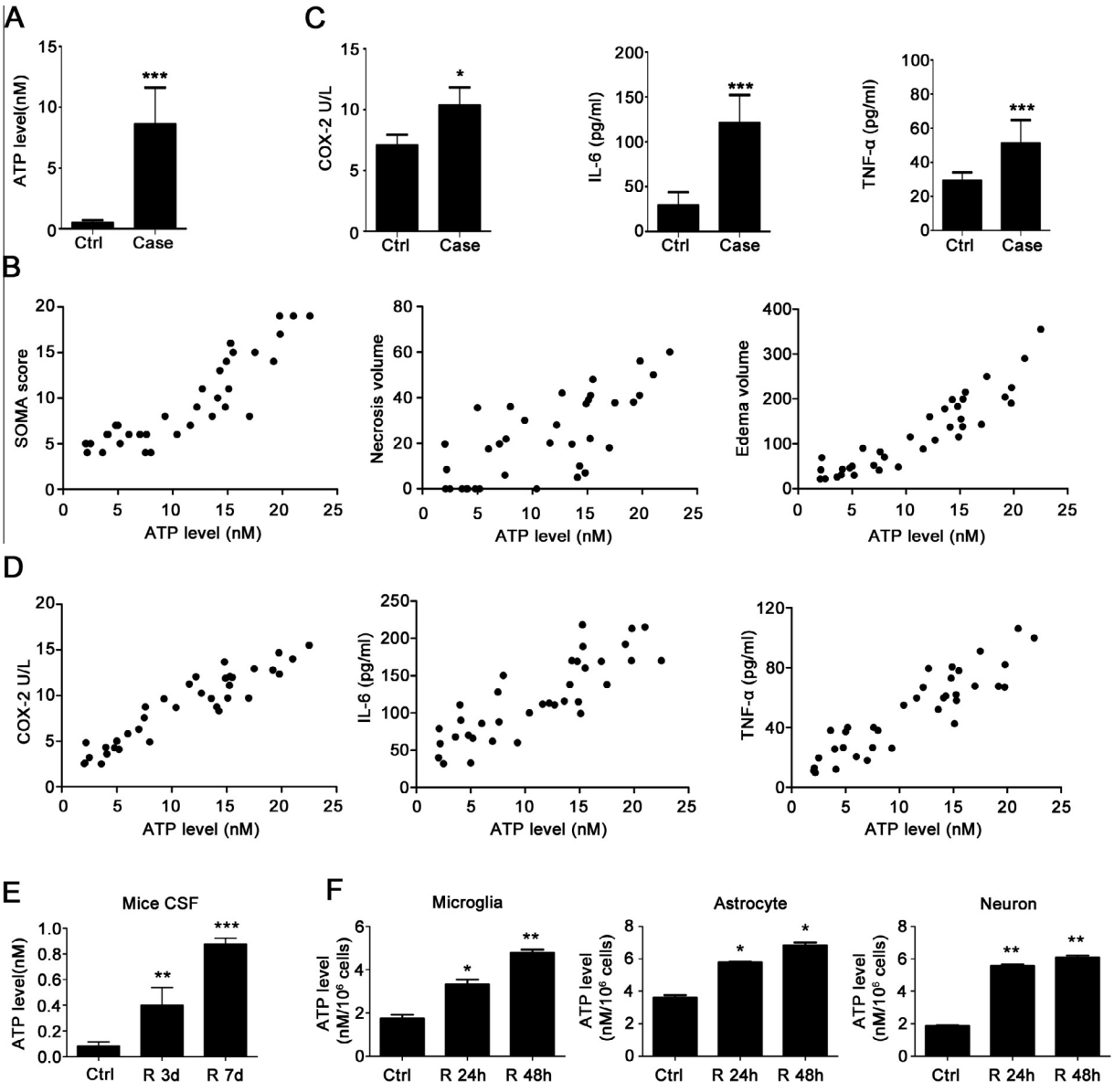

Fig. 1. Increased extracellular ATP (eATP) related to severity of radiation-induced brain injury (RBI). (A, C) Concentrations of ATP, COX-2, IL-6 and TNF-α in CSF of RBI patients (case group) and control people (control group), mean ± SEM (ATP: $t(35.075) = 10.310$, $P < 0.001$; COX-2: $t(89) = 2.120$, $P = 0.037$; IL-6: $t(38.514) = 10.091$, $P < 0.001$; TNF-α: $t(47.293) = 4.729$, $P < 0.001$. Student's t-test); $^{*}P < 0.05$ versus control group, $^{***}P < 0.001$ versus control group. (B) The SOMA score, edema and necrotic volume showed a positive correlation with eATP level. (D) The eATP level of case group showed a highly positive correlation with COX-2, IL-6 and TNF-α respectively. (E) In irradiated mice, the ATP levels in CSF at 3 and 7 days post-irradiation were shown as mean ± SEM; $n = 10$ ($F(2,27) = 209.297$, $P < 0.001$, ANOVA); $^{**}P < 0.01$ versus Ctrl, $^{***}P < 0.001$ versus Ctrl. (F) ATP levels in primary microglia, astrocytes and neurons at 24 and 48 h after radiation were shown as mean ± SEM; $n = 4$ (Microglia: $F(2,9) = 264.670$, $P < 0.001$, ANOVA. Astrocytes: $F(2,9) = 714.937$, $P < 0.001$, ANOVA. Neurons: $F(2,9) = 833.664$, $P < 0.001$, ANOVA); $^{*}P < 0.05$ versus Ctrl, $^{**}P < 0.01$ versus Ctrl.

increased the level of eATP in the supernatant after radiation (Fig. 1F). These data indicate that neurons and glial cells release ATP when damaged by radiation, and that elevated eATP is positively related to the severity of RBI.

3.2. ATP enhances microglial activity following radiation and amplifies the inflammatory response

Next, we examined whether the elevated eATP in RBI are merely a secondary response to radiation injury or an initiator that enhances microglial activity. Microglia were treated with radiation, ATP, or radiation plus ATP. Morphological changes were noted, and the percentages of activated microglia were quantified by CD11b staining. Resting microglia in control group had relatively small soma with thin protrusions; by contrast, microglia exposed to irradiation or exogenous ATP were activated with bigger soma, thicker but shorter protrusions and amoeboid morphology (Fig. 2A). Quantification of the activated microglia indicated that exposure to both radiation and ATP had an additive effect on microglial activation (Fig. 2B).

Next, the production of microglial inflammatory mediators in response to radiation and/or ATP was determined using ELISAs. We found that 10 μM ATP did not induce the release of all these inflammatory mediators. However, the combination of irradiation and 100 μM ATP caused a significant higher level of release of the inflammatory mediators than either treatment alone, indicating that ATP enhances the response of microglia to radiation stimulation and amplifies the release of inflammatory mediators such as COX-2, IL-6, and TNF-α (Fig. 2C). To determine whether ATP exacerbates neuronal injury after irradiation by activating

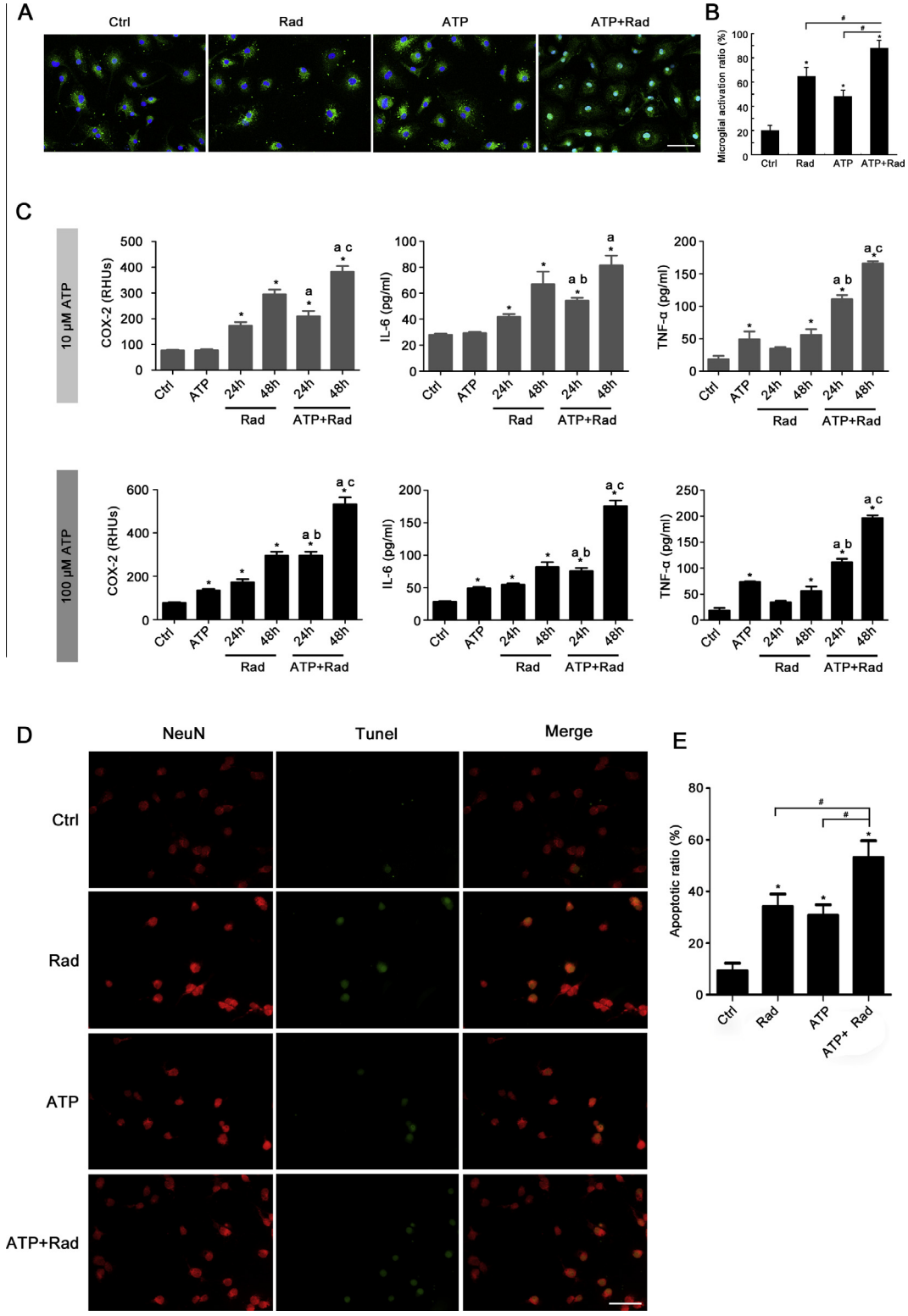

Fig. 2. ATP enhances microglial activity towards radiation and amplifies the inflammatory response. (A) Primary microglia were exposed to 10 Gy of radiation, then immunostained with CD11b antibody 24 h later. Representative images under indicated treatments were shown. Scale bar, 50 μm. (B) Statistical data of activated microglia were shown as mean ± SEM; $n = 6$ ($F(3,20) = 218.323$, $P < 0.001$, ANOVA); *, compared to control group, $P < 0.05$; $^{\#}$, compared to either ATP or radiation treated group, $P < 0.05$. (C) ELISA assays showed the alteration of inflammatory mediators in the supernatant of primary microglia at 24 h and 48 h under the treatment of ATP at 10 μM and 100 μM. Mean ± SEM; $n = 3$ (treatment of ATP at 10 μM, COX-2: $F(5,12) = 178.128$, $P < 0.001$; IL-6: $F(5,12) = 49.663$, $P < 0.001$; TNF-α: $F(5,12) = 180.759$, $P < 0.001$. Treatment of ATP at 100 μM, COX-2: $F(5,12) = 247.456$, $P < 0.001$; IL-6: $F(5,12) = 183.961$, $P < 0.001$; TNF-α: $F(5,12) = 412.903$, $P < 0.001$. ANOVA); $^{*}P < 0.05$, versus control group; a, versus ATP group, $P < 0.05$; b, versus radiation group, $P < 0.05$; c, versus radiation 48 h group, $P < 0.05$. (D) Neurons were co-cultured with control micorglia, irradiated microglia, 100 μM ATP or irradiated microglia treated with ATP. Neurons were then immunostained with NeuN antibody and apoptotic neurons were recognized through TUNEL staining. Representative images were shown. Scale bar, 50 μm. (E) The ratio of apoptotic neurons to live neurons (apoptotic ratio) was shown as mean ± SEM; $n = 6$ ($F(3,20) = 191.693$, $P < 0.001$, ANOVA); $^{*}P < 0.05$, versus control group; $^{\#}$, compared to either ATP or radiation treated group, $P < 0.05$.

microglia to release paracrine inflammatory factors, microglia were co-cultured with primary hippocampal neurons in a transwell system. Apoptotic neuronal cells were detected by double staining with NeuN and TUNEL. We found that the apoptosis ratio of neurons co-cultured with microglia exposed to both radiation and ATP was higher than that of neurons incubated with microglia that were irradiated or treated with ATP alone (Fig. 2D and E). These data indicate that irradiation induces direct injury of neurons and glial cells, leading to the release of ATP, which in turn enhances microglial activation, amplifies the production of inflammatory mediators, and aggravates radiation-induced neuronal injury.

3.3. Blockade of ATP–P2X7R mediated signaling reduces RBI

ATP activates purinergic receptors, including the seven P2XRs (P2X1-7R). To determine which of these receptors are involved in RBI, their mRNA expression levels were determined. The mRNAs encoding the P2X1R, P2X3R, P2X4R, and P2X7R were identified in both the control and radiation groups. We found that the levels of the mRNAs encoding P2X3R and P2X7R were upregulated significantly after irradiation, and the level of the mRNA encoding P2X7R was higher than that of the mRNA encoding P2X3R (Supplementary Fig. 1).

Considering the critical role of P2X7R in various brain injury (Skaper et al., 2006; Sperlagh and Illes, 2014), we hypothesized that the increased levels of ATP that occur after exposure to radiation might exacerbate brain injury through the P2X7R mediated signaling pathway. To confirm this hypothesis, we inhibited the P2X7R with BBG, a specific antagonist with low toxicity and high selectivity that can cross the blood–brain barrier (Diaz-Hernandez et al., 2009; Peng et al., 2009). Upon exposure to radiation, the level of P2X7R staining increased accompanied by change in morphology of the cells to amoeboid phenotype. Incubation of the cells with BBG (1 μM) prior to irradiation attenuated the increased P2X7R expression and morphological transformations significantly, indicating the inhibition of microglial activation (Fig. 3B).

Our previous study found that neuronal progenitor cells, which contribute to tissue repair by promoting neurogenesis, were depleted after RBI, and their differentiation into neurons was inhibited via microglia-mediated inflammatory mechanisms (Peng et al., 2014). Using a similar methodology, we evaluate the role of the ATP–P2X7R mediated signaling during RBI *in vivo*. Neuronal numbers in the cortex and neuronal proliferation in the dentate gyrus were evaluated in mice following 14 days of whole brain irradiation. Beta-tubulin staining revealed that the number of neurons in the cortex was reduced after irradiation (Fig. 3C and D). Moreover, the number of $BrdU^+/NeuN^+$ cells in the dentate gyrus was also reduced significantly after irradiation (Fig. 3E and F). Administration of BBG attenuated the irradiation-induced losses of neurons in the cortex and $BrdU^+/NeuN^+$ neural progenitor cells in the dentate gyrus (Fig. 3C–F). These results demonstrate that exposure to radiation induces neuronal injury and decreases neuronal proliferation by activating microglia through the ATP–P2X7R pathway.

To evaluate the contribution of the ATP–P2X7R mediated signaling in causing neurological deficits in RBI, the spatial learning and memory of mice were determined at 8 weeks post-irradiation using a Morris water maze. Consistent with previous studies (Ben Abdallah et al., 2013; Peng et al., 2014), the latency and path length to find a hidden platform were longer in irradiated mice than in control mice (Fig. 3G and H). The latencies and path lengths of irrradiated mice treated with BBG were significantly shorter than those of mice exposed to radiation alone, but longer than those of control mice. On day 7 of the experiment, BBG-treated mice spent significantly more time in the target quadrant of the water maze than irradiated mice ($P < 0.05$), suggesting an improved spatial memory (Fig. 3I and J). These data indicate that inhibition of the ATP–P2X7R mediated signaling can improve spatial memory and reduce neurological deficits caused by RBI.

3.4. Radiation-induced microglial paracrine signaling is mediated by P2X7R in vitro

Next, we examined the mechanisms underlying the ATP–P2X7R mediated signaling pathway in RBI. We first tested whether inhibition of the P2X7R would suppress radiation-induced production of inflammation mediators. Indeed, BBG inhibited the upregulation of mRNA expression levels COX-2, IL-6, and TNF-α after exposure of primary microglia to radiation (Fig. 4A). In addition, we found that the mRNA level of P2X7R was also upregulated in response to irradiation, and this upregulation was attenuated by BBG at both the 24 h and 48 h time points (Fig. 4B). These results indicate that the P2X7R not only mediates radiation-induced activation of microglia, but also regulates the secretion of inflammatory mediators. Consistently, our Western blot results further confirmed that radiation significantly upregulated the protein expressions of both P2X7R and COX-2 (Fig. 4C). Together, these results indicate a specific role of the P2X7R in microglial activation and secretion of inflammatory mediators induced by radiation.

To exclude any unknown side effects of pharmacological inhibitors, we used the P2X7R knockdown via RNA interference. We found that upregulation of P2X7R mRNA was inhibited significantly by transfection of the microglia with a P2X7R-specific siRNA at 24 h or 48 h after irradiation (Fig. 5A). Moreover, irradiation-induced upregulation of COX-2, IL-6 and TNF-α were also markedly suppressed at 48 h time point (Fig. 5B). Consistently, Western blots showed P2X7R and COX-2 protein were upregulated after radiation and were then inhibited by P2X7R knockdown at various time point (Fig. 5C, upper panel). Taken together, these data provide crucial evidence that the P2X7R is involved in microglial paracrine signaling after radiation, indicating a feedback loop in microglial activation during RBI.

3.5. Radiation-induced microglial paracrine signaling is mediated by P2X7R in vivo

Next, we examined the role of the P2X7R in microglial activation and paracrine signaling *in vivo*. We found that the colocalized immune-expressions of IBA-1, a marker for microglia and P2X7R were remarkably upregulated in irradiated mice (Fig. 6A and B). Treatment with BBG significantly decreased the number of activated $IBA1^+$ microglia. Irradiation also induced a time-dependent elevation in the mRNA expression levels of P2X7R (Fig. 6C) and proinflammatory mediators (Fig. 6D). BBG could suppress these upregulation mainly at 7 days after irradiation (Fig. 6C and D). Consistently, radiation markedly augmented the protein expression of P2X7R and COX-2, which could be inhibited by BBG 7 days after treatment (Fig. 6E). These results confirm that the P2X7R is involved in activation and paracrine signaling of irradiated microglia *in vivo*, suggesting that the P2X7R mediates the radiation-induced release of proinflammatory mediators, including COX-2, IL-6, and TNF-α, *in vivo*.

3.6. Pathways involved in P2X7R-mediated microglial activation and paracrine signaling in RBI

To explore the possible mechanisms involved in the P2X7R-mediated microglial activation and paracrine signaling in RBI, the nuclear factor κB (NF-κB) and PI3K/AKT transduction pathways in the diverse cascades of inflammation were examined.

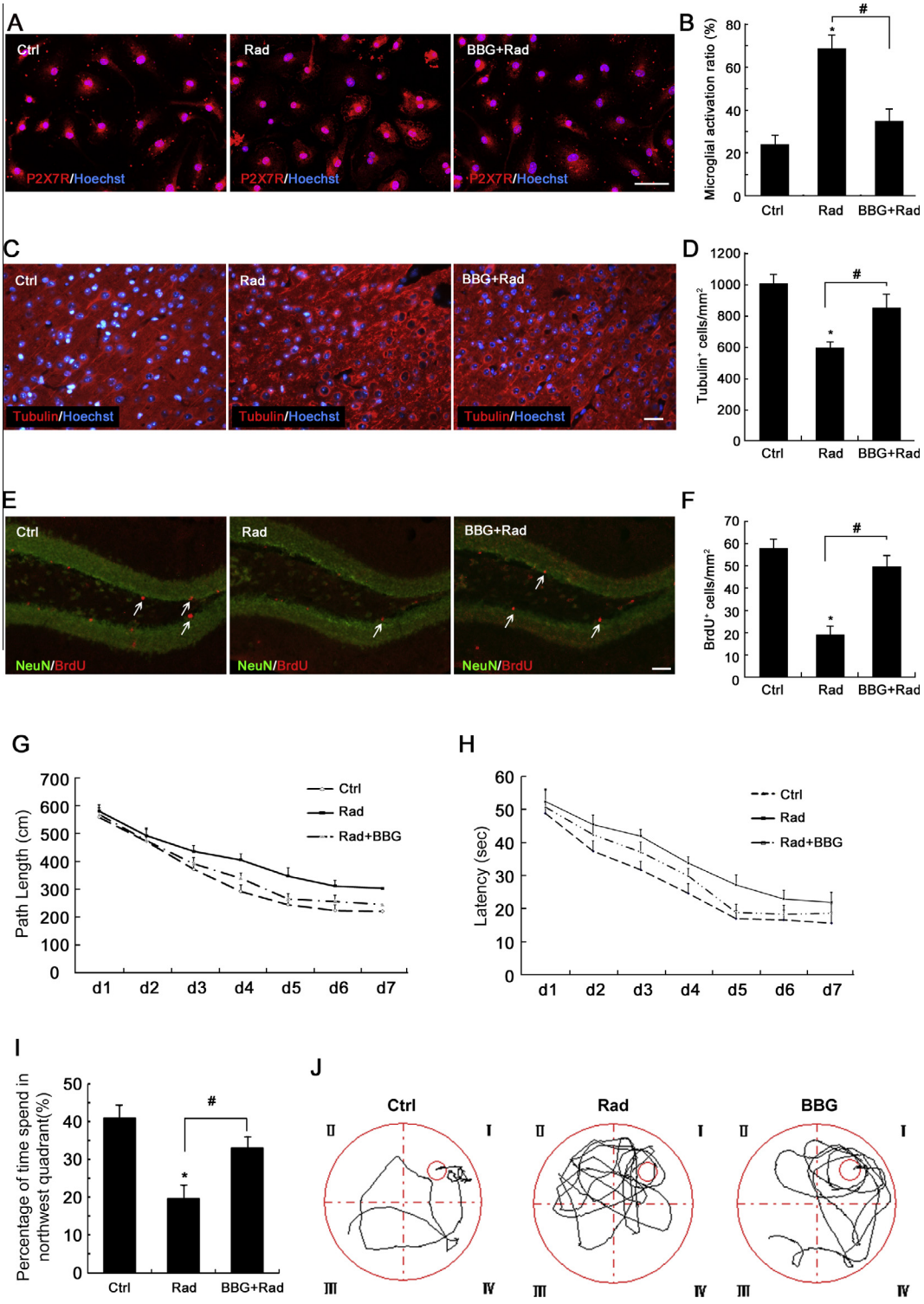

Fig. 3. P2X7R is involved in RBI both *in vitro* and *in vivo*. (A) Primary microglia exposed to single dose of radiation (10 Gy), or pre-treated with BBG (1 μM) for 1 h before radiation. Cells were immunostained with P2X7R antibody (green). Representative images were shown (scale bar is 50 μm). (B) Statistical percentages of activated microglia were shown as mean ± SEM: $n = 6$ ($F(2,15) = 414.764$, $P < 0.001$, ANOVA). (C) Representative sections from cortex immunostained with anti-beta tubulin (red) and Hoechst 33258 (blue). Scale bar is 20 μm. (D) Quantification of viable neurons in layer-3 cortex were shown as mean ± SEM; $n = 5$ ($F(2,12) = 85.521$, $P < 0.001$, ANOVA). (E) Representative sections from hippocampus immunostained with anti-NeuN (green) and anti-BrdU (red) antibodies. Scale bar is 50 μm. Statistical data were shown in (F). Quantitative analysis showed decreased numbers of $BrdU^+/NeuN^+$ NPCs 14 days after irradiation and a restoration using BBG. Data were shown as mean ± SEM; $n = 5$ ($F(2,12) = 171.068$, $P < 0.001$, ANOVA). (G) The swim path and (H) the latency length before arrival on the platform were recorded for 7 consecutive days in each group. (I) Percentage of time in the northwest quadrant of the water maze for mice in each group. The difference between different groups was assessed using probe trials on day 7 of training and was analyzed using a 1-way ANOVA followed by Bonferroni's test, $n = 6$ ($F(2,15) = 127.081$, $P < 0.001$, ANOVA). (J) Swimming trail of each group in probe trial was recorded by DMS-2. $^*P < 0.05$, versus control group; $^\#$, versus radiation group, $P < 0.05$. (For interpretation of the references to color in this figure legend, the reader is referred to the web version of this article.)

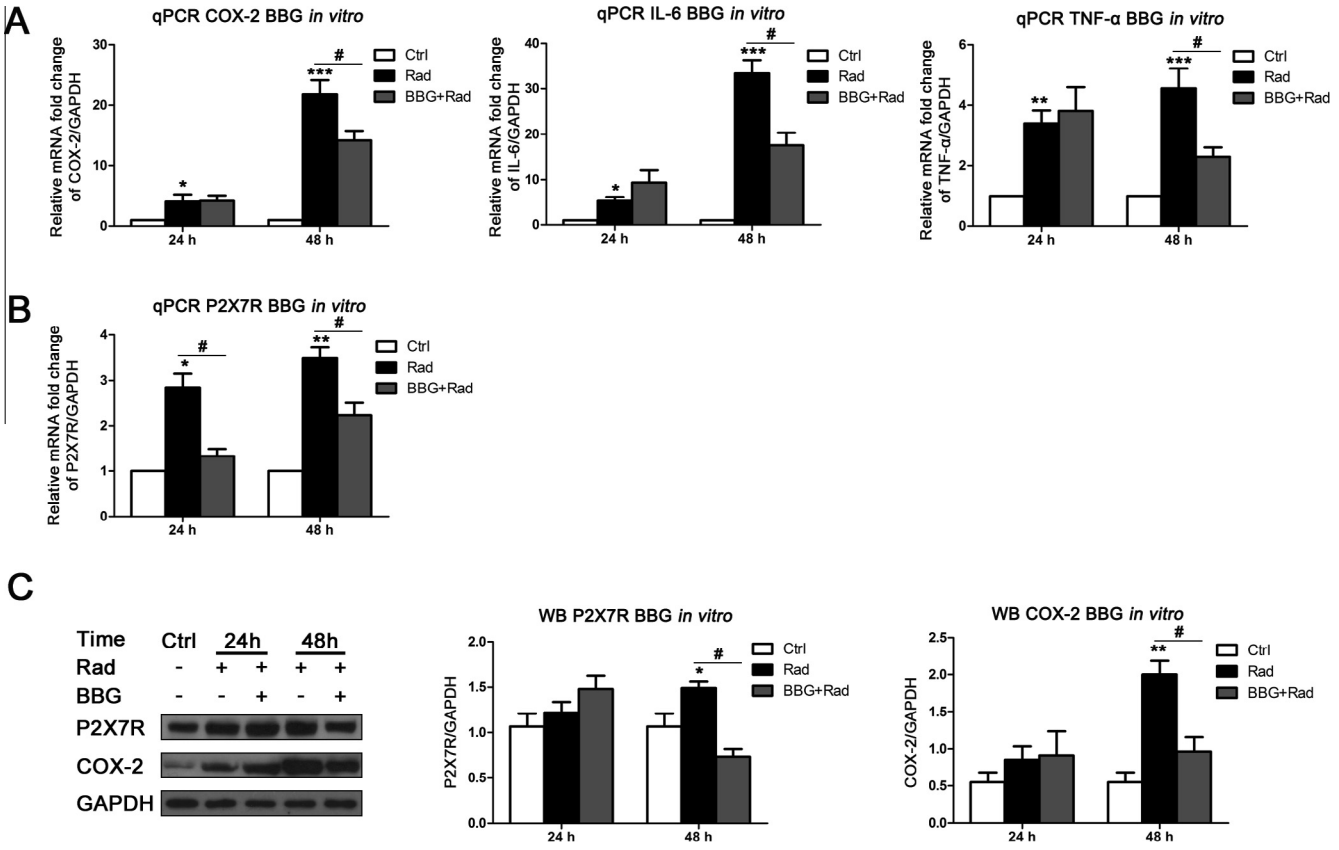

Fig. 4. Pharmacological inhibition of P2X7R suppresses radiation induced microglial paracrine signaling. Quantitive real-time PCRs of COX-2, IL-6, TNF-α (A) and P2X7R (B) in primary microglial cells were performed at 24 h or 48 h post irradiation in indicated groups. Data from control group were set to 100% for normalization. Statistical data were shown as the mean ± SEM; $n = 3$ (COX-2: $F_{24h}(2,6) = 12.885$, $P = 0.007$; $F_{48h}(2,6) = 122.267$, $P < 0.001$. IL-6: $F_{24h}(2,6) = 19.116$, $P = 0.002$; $F_{48h}(2,6) = 140.384$, $P < 0.001$. TNF-α: $F_{24h}(2,6) = 10.086$, $P = 0.012$; $F_{48h}(2,6) = 52.530$, $P < 0.001$. P2X7R: $F_{24h}(2,6) = 19.040$, $P = 0.003$; $F_{48h}(2,6) = 62.029$, $P < 0.001$. ANOVA). (C) Cells lysates with the same treatments as in (A) were subjected to Western blot for P2X7R and COX-2. Representative blots of three independent experiments were shown on the left panel, and the densitometric analysis were shown on the right panel. Mean ± SEM; $n = 3$ (P2X7R: $F_{24h}(2,6) = 3.284$, $P = 0.109$; $F_{48h}(2,6) = 38.913$, $P < 0.001$. COX-2: $F_{24h}(2,6) = 2.188$, $P = 0.193$; $F_{48h}(2,6) = 56.210$, $P < 0.001$. ANOVA). *, Compared to control group, $P < 0.05$; **, compared to control group, $P < 0.01$; ***, compared to control group, $P < 0.001$; #, compared to radiation treated group, $P < 0.05$.

Indeed we found that the phosphorylation of P65 was upregulated after irradiation of primary microglia, and this effect was inhibited by BBG pre-incubation (Fig. 7A). The same trend was also observed for the expression levels of COX-2 and the P2X7R. To test whether NF-κB is the upstream for COX-2 expression, a NF-κB pathway specific inhibitor pyrrolidine dithiocarbamate (PDTC) was used (Liu et al., 1999). While PDTC had no effect on the expression level of the P2X7R, it significantly reversed the irradiation-induced COX-2 upregulation and phosphorylated P65. These findings indicate that P2X7R activation induces the NF-κB transduction pathway which is required for COX-2 production after irradiation.

Next, we determined whether the PI3K/AKT pathway is engaged in radiation-induced microglial paracrine signaling. We found that the expression level of p-AKT was upregulated after irradiation and attenuated by BBG pre-incubation (Fig. 7B). LY294002, a specific inhibitor of PI3K (Liu et al., 2010), had an inhibitory effect on the radiation-induced enhancements of p-AKT and COX-2, but had no effect on the expression level of the P2X7R (Fig. 7B). These results suggest that the PI3K/AKT transduction pathway participates in the paracrine signaling of microglia activated by radiation, and that the P2X7R is an upstream activator of this pathway. Overall, the data indicate that both the NF-κB and PI3K/AKT signaling pathways are involved in the activation and paracrine signaling of irradiated microglia after P2X7 receptor activation.

4. Discussion

Communication between microglia and neurons in many pathological cascades involves eATP (Ekdahl et al., 2009). Here, we report that elevated eATP is positively related to the severity of RBI and the levels of inflammatory mediators (COX-2, IL-6, and TNF-α) in CSF of patients. We also show that radiation-induced the release of ATP from cultured neuronal/glial cells and also in the CSF of irradiated mice. The elevated eATP activates P2X7 receptor to enhance microglial activity and amplifies the production of inflammatory mediators, leading to aggravation of neuronal injury. Pharmacological or genetic blockade of the P2X7R suppressed the radiation-induced secretion of inflammatory mediators by microglia, promoted cell proliferation in the dentate gyrus, and improved the spatial learning of irradiated mice. Finally we found that the NF-κB and PI3K/AKT signaling pathways are critical for P2X7R-dependent microglial activation and the subsequent production of inflammatory mediators. These data demonstrate that the ATP–P2X7R axis is engaged in a self-perpetuating neurotoxicity cycle between microglia and neurons, and thus contributes to the pathogenesis of radiation encephalopathy (Fig. 8). In this vicious cycle, neuronal cells injured by ionizing radiation release ATP, which triggers microglia to produce inflammatory mediators which further exacerbates the neuronal injury and other pathophysiologic processes. Therefore, blockade of P2X7R by the specific

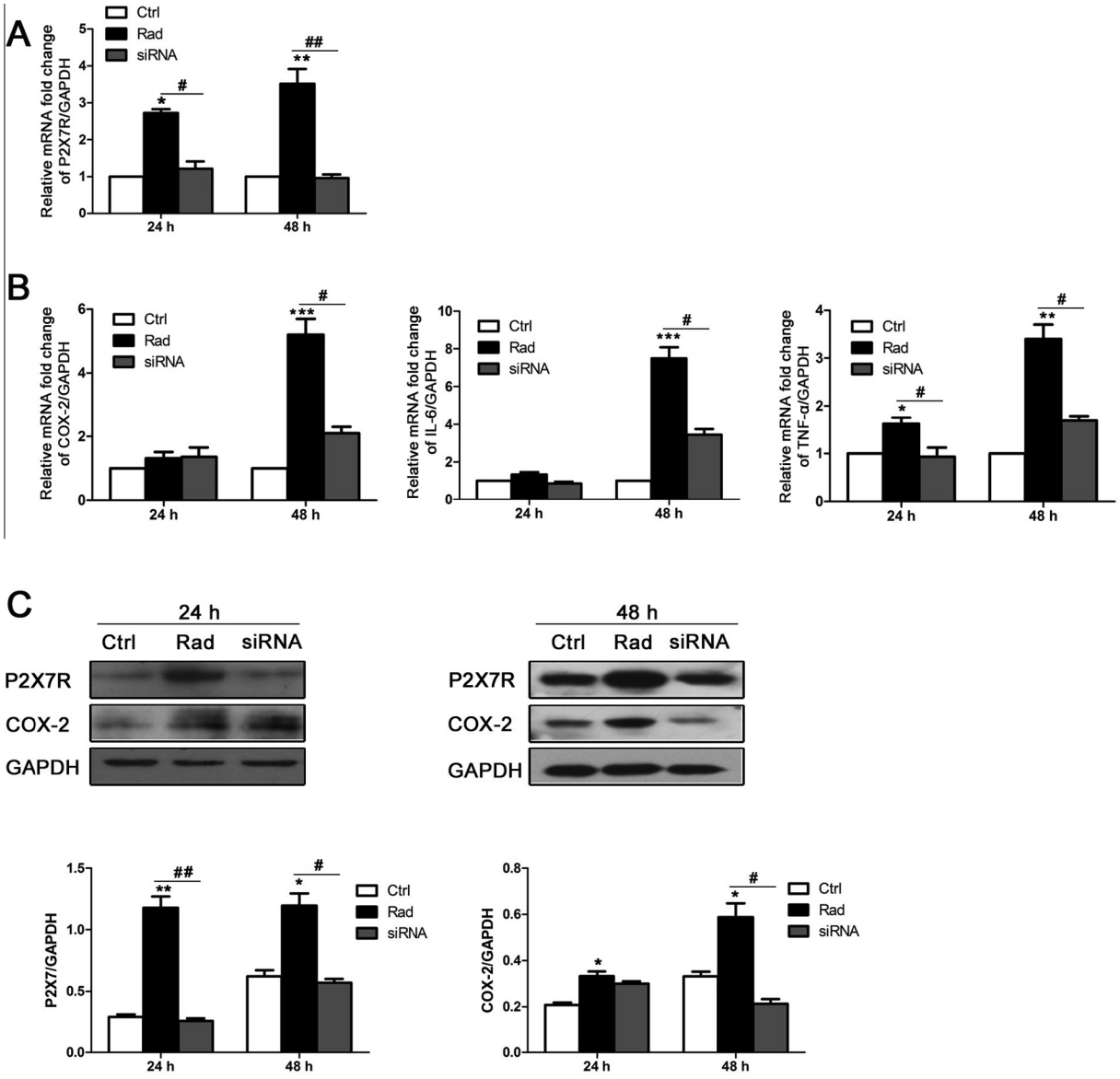

Fig. 5. Genetic knockdown of P2X7R suppresses radiation induced microglial paracrine signaling. Cells treatment as in Fig. 4 were transfected with P2X7R siRNA fragments. Real-time PCRs were performed to detect the mRNA levels of P2X7R (A), COX-2, IL-6 and TNF-α (B). Mean ± SEM; $n = 3$ (P2X7R: $F_{24h}(2,6) = 162.071$, $P < 0.001$; $F_{48h}(2,6) = 113.515$, $P < 0.001$. COX-2: $F_{24h}(2,6) = 2.624$, $P = 0.152$; $F_{48h}(2,6) = 146.905$, $P < 0.001$. IL-6: $F_{24h}(2,6) = 5.088$, $P = 0.051$; $F_{48h}(2,6) = 215.095$, $P < 0.001$. TNF-α: $F_{24h}(2,6) = 21.584$, $P = 0.002$; $F_{48h}(2,6) = 137.090$, $P < 0.001$. ANOVA). (C) Primary microglia treated as in (A) were subjected to Western blot. The protein expression levels of P2X7R and COX-2 were shown on the upper panel and the densitometric analysis on the bottom. Mean ± SEM; $n = 3$ (P2X7R: $F_{24h}(2,6) = 274.422$, $P < 0.001$; $F_{48h}(2,6) = 80.972$, $P < 0.001$ .COX-2: $F_{24h}(2,6) = 21.157$, $P = 0.002$; $F_{48h}(2,6) = 75.182$, $P < 0.001$. ANOVA). *, Compared to control group, $P < 0.05$; **, compared to control group, $P < 0.01$; ***, compared to control group, $P < 0.001$; $^{\#}$, compared to radiation treated group, $P < 0.05$; $^{\#\#}$, compared to radiation treated group, $P < 0.01$.

antagonist BBG might represent a new strategy to alleviate RBI. To our knowledge, this is the first study to investigate the underling mechanism of P2X7R involvement in RBI, and the potential therapeutic effect of BBG targeting P2X7R.

P2X7R, as an ionotropic P2 receptor, is implicated in several CNS disorders, such as lipopolysaccharide-induced inflammatory responses (Bernardino et al., 2008), neuronal damage in the rat striatum (Carmo et al., 2014), amyotrophic lateral sclerosis (Gandelman et al., 2010), Alzheimer's disease (Lee et al., 2011), spinal cord injury (Peng et al., 2009; Wang et al., 2004) and stroke (Lammer et al., 2011). These studies indicate that microglial P2X7R is a master hub for microglia activation and neuroinflammation, indicating P2X7R to be a potent therapeutic target for various neurological diseases (Skaper et al., 2006; Sperlagh and Illes, 2014). OxATP and PPADS, two firstly reported P2X7R antagonists, were reported to be neuroprotective (Wang et al., 2004). However, oxATP and PPADS are nonselective, and their actions cannot be reliably attributed to P2X7R blockade. Then BBG, an analog of FD&C blue dye, a more selective antagonist of P2X7R was found to reduce neuronal injury (Cotrina and Nedergaard, 2009; Jiang et al., 2000; Peng et al., 2009). Studies showed that BBG suppresses the inflammatory response mediated by P2X7R and inhibits downstream events such as membrane blebbing and endocytosis of the cationic dye YOPRO-1 (Jiang et al., 2000). Consistently, blockade of P2X7R by BBG prevented ATP excitotoxicity in mice (Matute et al., 2007; Sharp et al., 2008). In addition, BBG has been shown to improve the functional and histopathological consequences of spinal cord injury in rat models (Peng et al., 2009; Wang et al., 2004). However, Alexander and colleagues failed to repeat these results when trying to assess the consideration of clinical testing using selective P2X7R antagonists (Marcillo et al., 2012). Since the dosing schedule of BBG in the spinal cord injury model of

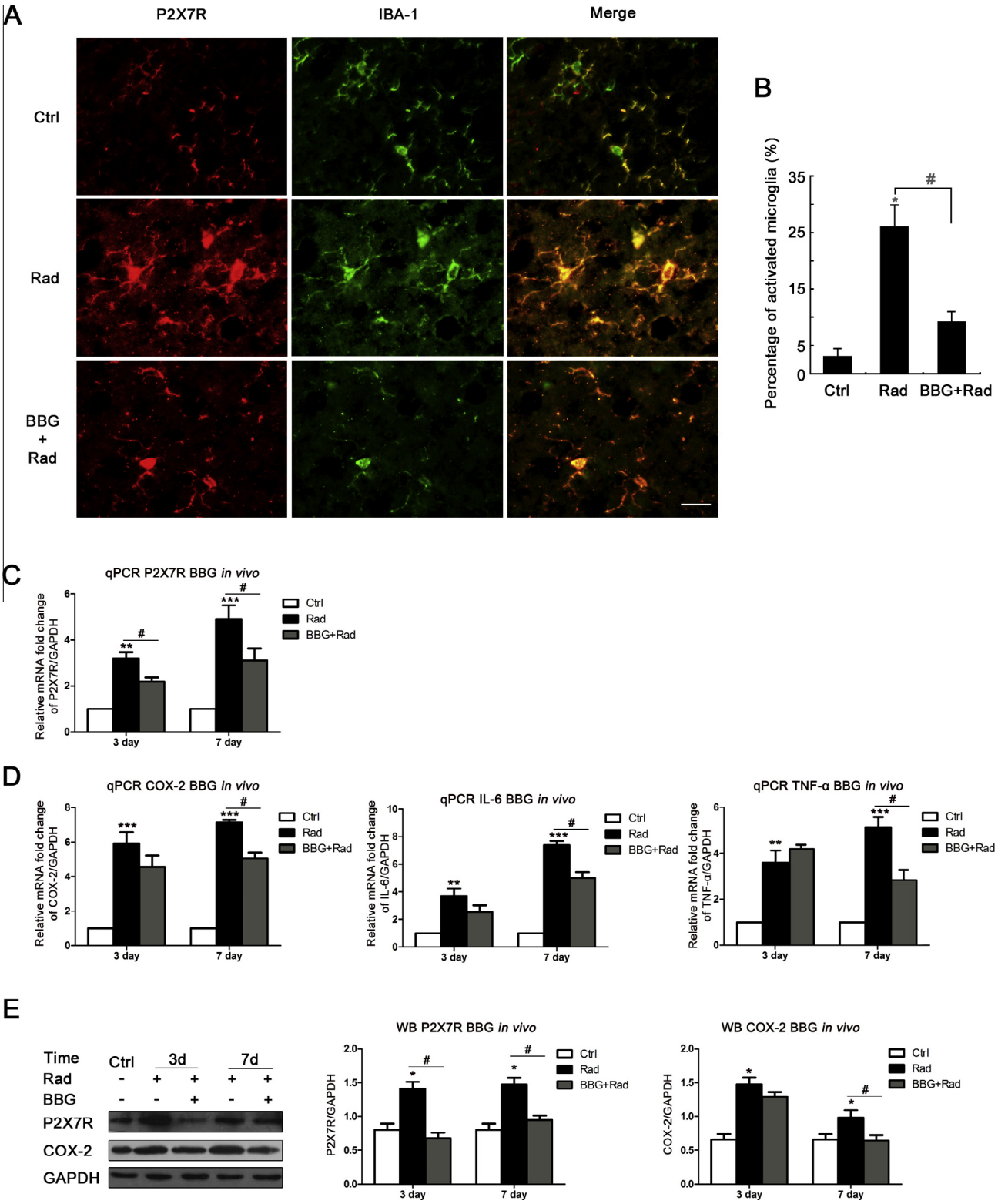

Fig. 6. P2X7R is involved in radiation induced microglia activation *in vivo*. (A) Mice were treated as mentioned in the material and methods section. Double-immunofluorescence staining of the cortex with IBA1 for microglia (green) and P2X7R (red) were shown (scale bar 20 μm). (B) Statistical percentage of P2X7R colocalized with IBA1 were shown as mean ± SEM; $n = 6$ ($F(2,15) = 1554.729$, $P < 0.001$, ANOVA). mRNA levels of P2X7R (C) and COX-2, IL-6 and TNF-α (D) of the whole brain lysates from irradiated mice were shown by using the real-time PCR assays. GAPDH was used as an internal control. Mean ± SEM; $n = 3$ (P2X7R: $F_{3d}(2,6) = 108.085$, $P < 0.001$; $F_{7d}(2,6) = 55.677$, $P < 0.001$. COX-2: $F_{3d}(2,6) = 66.883$, $P < 0.001$; $F_{7d}(2,6) = 650.170$, $P < 0.001$. IL-6: $F_{3d}(2,6) = 33.269$, $P = 0.001$; $F_{7d}(2,6) = 329.607$, $P < 0.001$. TNF-α: $F_{3d}(2,6) = 64.045$, $P < 0.001$; $F_{7d}(2,6) = 46.800$, $P < 0.001$. ANOVA). (E) Mice were treated with or without BBG administration for 3 or 7 days post-irradiation. Then the brain lysates were subjected to Western blot assays to show the protein alteration of P2X7R and COX-2. The bar graph showed the statistical results of Western blots. Mean ± SEM; $n = 3$ (P2X7R: $F_{3d}(2,6) = 13.193$, $P = 0.006$; $F_{7d}(2,6) = 39.367$, $P < 0.001$. COX-2: $F_{3d}(2,6) = 50.477$, $P < 0.001$; $F_{7d}(2,6) = 13.290$, $P = 0.006$. ANOVA). *, Compared to control group, $P < 0.05$; **, compared to control group, $P < 0.01$; ***, compared to control group, $P < 0.001$; $^{\#}$, compared to radiation treated group. (For interpretation of the references to color in this figure legend, the reader is referred to the web version of this article.)

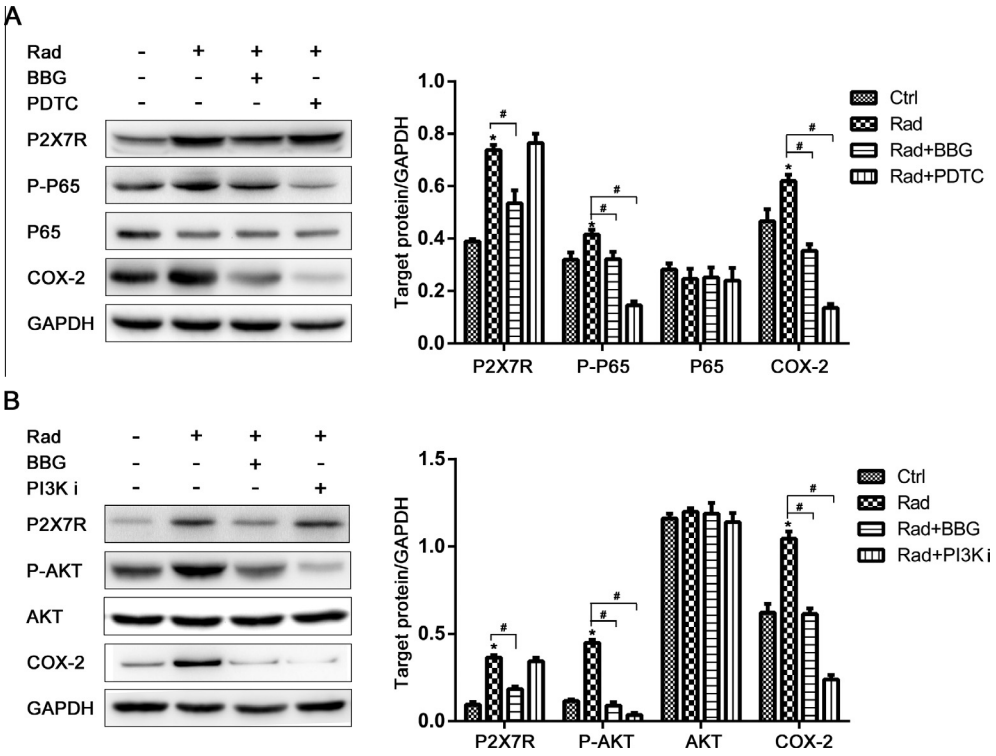

Fig. 7. NF-κB and PI3K/AKT pathways are involved in microglial activation and paracrine signaling in RBI. (A) Primary microglia pretreated with BBG (1 μM) or PDTC for 60 min were exposed to radiation at 10 Gy. Protein expressions of P-P65, P65, P2X7R and COX-2 were determined by Western blots. The expression of GAPDH was served as an internal control. The statistical data of each protein versus GAPDH were shown on the right panel as mean ± SEM; $n = 3$ (P2X7R: $F(3,8) = 89.387$, $P < 0.001$; P-P65: $F(3,8) = 72.480$, $P < 0.001$; P65: $F(3,8) = 0.715$, $P = 0.570$; COX-2: $F(3,8) = 141.643$, $P < 0.001$. ANOVA). (B). Cells lysates were subjected to Western blots with anti-p-AKT, AKT, P2X7R and COX-2 antibodies. The expression of GAPDH was served as an internal control. The statistical data were shown as mean ± SEM; $n = 3$ (P2X7R: $F(3,8) = 199.603$, $P < 0.001$; P-AKT: $F(3,8) = 569.204$, $P < 0.001$; AKT: $F(3,8) = 1.149$, $P = 0.387$; COX-2: $F(3,8) = 210.079$, $P < 0.001$. ANOVA). *, Compared to control group, $P < 0.05$; #, compared to radiation treated group, $P < 0.05$.

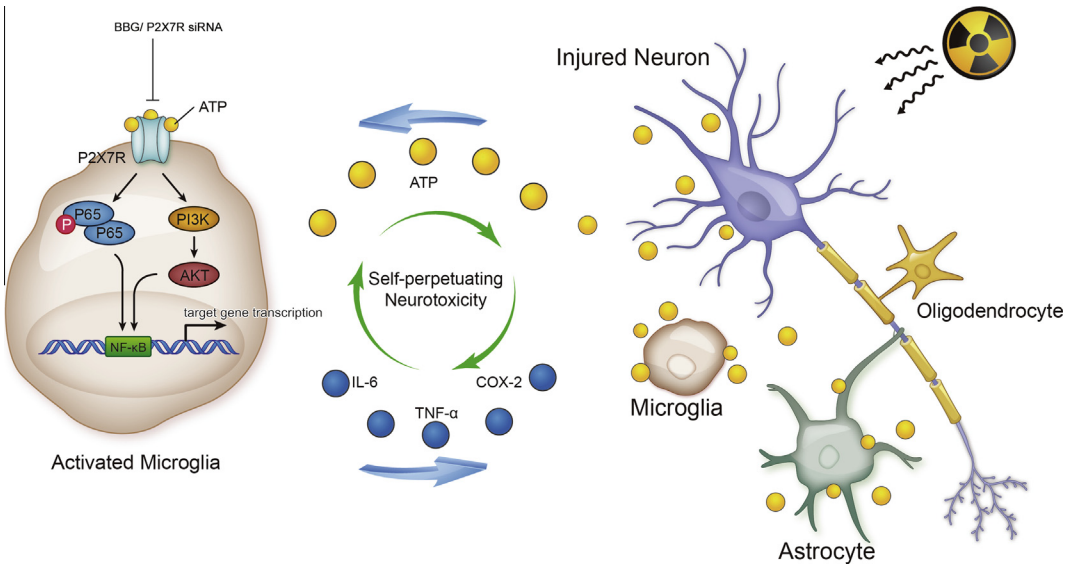

Fig. 8. Schematic representation of neurotoxicity cycle mediated by ATP and P2X7R in RBI. Injured neurons under radiation release large amount of extracellular ATP (eATP). eATP, through P2X7R, further activates microglia and induces the release of inflammatory mediators such as COX-2, IL-6 and TNF-α, which exacerbates neuronal injury and other pathophysiologic process. Pharmacological or genetic inhibition of ATP-P2X7 axis restores neuronal cell proliferation and alleviate RBI.

Peng's study is relatively short (BBG at 10 or 50 mg/kg, start right after injury and once daily on days 2 and 3), a longer duration of dosing is recommended to achieve a robust effect. In addition, this divergence implies that the potentially exciting therapies require further preclinical investigations before the implementation in human clinical trials targeting P2X7 receptors. In our current study, the BBG scheme was relatively long (50 mg/kg, started before radiation and continued once daily for seven consecutive

days). In line with the neuroprotective potential of BBG, we found that BBG inhibits microglial activation and paracrine signaling, thereby alleviating radiation encephalopathy.

Study showed that P2X7R channel allows Ca^{2+} influx and K^+ outflow when activated by ATP. The elevation of Ca^{2+} through P2X7R is important for NF-κB and PI3K/AKT transduction pathways (Potucek et al., 2006). Kaya and colleague reported that ATP selectively suppresses the synthesis of the inflammatory protein MRF-1 through Ca^{2+} influx via P2X7R in cultured microglia (Kaya et al., 2002). Indeed, we found that inhibition of P2X7R inactivated NF-κB and PI3K/AKT cascade associated with RBI. But, how the P2X7R-mediated Ca^{2+} influx and K^+ outflow regulates the internal molecular functions under RBI remains obscure, and is worthy of further investigation.

Despite the optimistic efficacy of P2X7 antagonists in pre-clinical studies, it has yet to be determined whether these P2X7 antagonists will translate into positive clinical outcomes. The pioneering developments of P2X7R antagonists, such as CE-224,535 (Stock et al., 2012) and AZD-9056 (Keystone et al., 2012) have been entered Phase II trials in rheumatoid arthritis patients. Considering the acceptable safety and tolerability profile of these antagonists, it is possible to develop P2X7R-targeting compounds in CNS disorders. The absence or low expression of P2X7Rs in healthy tissue limits systemic side effects of these compounds and although the majority of known antagonists fails to pass the blood–brain barrier, BBG and some new antagonists readily enter the CNS (Bhattacharya et al., 2013). Thus, modulators of P2X7R may become important therapeutic tools (Sperlagh and Illes, 2014).

In conclusion, our study describes the relevance of eATP-induced microglial activation and release of inflammatory mediators during RBI. The mechanisms involve the activation of the P2X7R, NF-κB and PI3K/AKT signaling pathways in microglia, initiation of a secondary inflammatory response and subsequently leading to neuronal damage. These findings have significant clinical implications for the treatment of RBI; specifically, blockade of P2X7R breaks the neurotoxic cycle between neurons and microglia, thereby diminishing excessive brain injury and improving outcomes after radiation.

Acknowledgments

The authors declare no conflict of interest. This work was supported by National Natural Science Foundation of China (Nos. 81272576, 81471249), the Fundamental Research Funds for the Central Universities and Funds for Pearl River Science & Technology Star of Guangzhou City (2012J2200088), Program for New Century Excellent Talents in University (NCET-13-0612), Elite Young Scholars Program of Sun Yat-Sen Memorial Hospital (Y201402) to Y.T., and by National Institute of Health (R01NS088627) to L.J.W.

Appendix A. Supplementary data

Supplementary data associated with this article can be found, in the online version, at http://dx.doi.org/10.1016/j.bbi.2015.06.020.

References

Ben Abdallah, N.M., Filipkowski, R.K., Pruschy, M., Jaholkowski, P., Winkler, J., Kaczmarek, L., Lipp, H.P., 2013. Impaired long-term memory retention: common denominator for acutely or genetically reduced hippocampal neurogenesis in adult mice. Behav. Brain Res. 252, 275–286.

Bernardino, L., Balosso, S., Ravizza, T., Marchi, N., Ku, G., Randle, J.C., Malva, J.O., Vezzani, A., 2008. Inflammatory events in hippocampal slice cultures prime neuronal susceptibility to excitotoxic injury: a crucial role of P2X7 receptor-mediated IL-1beta release. J. Neurochem. 106, 271–280.

Bhattacharya, A., Wang, Q., Ao, H., Shoblock, J.R., Lord, B., Aluisio, L., Fraser, I., Nepomuceno, D., Neff, R.A., Welty, N., Lovenberg, T.W., Bonaventure, P., Wickenden, A.D., Letavic, M.A., 2013. Pharmacological characterization of a novel centrally permeable P2X7 receptor antagonist: JNJ-47965567. Br. J. Pharmacol. 170, 624–640.

Carmo, M.R., Menezes, A.P., Nunes, A.C., Pliassova, A., Rolo, A.P., Palmeira, C.M., Cunha, R.A., Canas, P.M., Andrade, G.M., 2014. The P2X7 receptor antagonist Brilliant Blue G attenuates contralateral rotations in a rat model of Parkinsonism through a combined control of synaptotoxicity, neurotoxicity and gliosis. Neuropharmacology 81, 142–152.

Chen, Z., Palmer, T.D., 2013. Differential roles of TNFR1 and TNFR2 signaling in adult hippocampal neurogenesis. Brain Behav. Immun. 30, 45–53.

Cheng, R.D., Ren, J.J., Zhang, Y.Y., Ye, X.M., 2014. P2X4 receptors expressed on microglial cells in post-ischemic inflammation of brain ischemic injury. Neurochem. Int. (Epub ahead of print)

Choi, D.K., Koppula, S., Suk, K., 2011. Inhibitors of microglial neurotoxicity: focus on natural products. Molecules 16, 1021–1043.

Cotrina, M.L., Nedergaard, M., 2009. Physiological and pathological functions of P2X7 receptor in the spinal cord. Purinergic Signal 5, 223–232.

Diaz-Hernandez, M., Diez-Zaera, M., Sanchez-Nogueiro, J., Gomez-Villafuertes, R., Canals, J.M., Alberch, J., Miras-Portugal, M.T., Lucas, J.J., 2009. Altered P2X7-receptor level and function in mouse models of Huntington's disease and therapeutic efficacy of antagonist administration. FASEB J. 23, 1893–1906.

Dietrich, J., Monje, M., Wefel, J., Meyers, C., 2008. Clinical patterns and biological correlates of cognitive dysfunction associated with cancer therapy. Oncologist 13, 1285–1295.

Ekdahl, C.T., Kokaia, Z., Lindvall, O., 2009. Brain inflammation and adult neurogenesis: the dual role of microglia. Neuroscience 158, 1021–1029.

Engel, T., Gomez-Villafuertes, R., Tanaka, K., Mesuret, G., Sanz-Rodriguez, A., Garcia-Huerta, P., Miras-Portugal, M.T., Henshall, D.C., Diaz-Hernandez, M., 2012. Seizure suppression and neuroprotection by targeting the purinergic P2X7 receptor during status epilepticus in mice. FASEB J. 26, 1616–1628.

Ferguson, K.J., Wardlaw, J.M., Edmond, C.L., Deary, I.J., Maclullich, A.M., 2005. Intracranial area: a validated method for estimating intracranial volume. J. Neuroimaging 15, 76–78.

Fields, R.D., Stevens, B., 2000. ATP: an extracellular signaling molecule between neurons and glia. Trends Neurosci. 23, 625–633.

Gandelman, M., Peluffo, H., Beckman, J.S., Cassina, P., Barbeito, L., 2010. Extracellular ATP and the P2X7 receptor in astrocyte-mediated motor neuron death: implications for amyotrophic lateral sclerosis. J. Neuroinflammation 7, 33.

Genc, M., Genc, E., Genc, B.O., Kiresi, D.A., 2006. Significant response of radiation induced CNS toxicity to high dose steroid administration. Br. J. Radiol. 79, e196–199.

Gonzalez-Scarano, F., Baltuch, G., 1999. Microglia as mediators of inflammatory and degenerative diseases. Annu. Rev. Neurosci. 22, 219–240.

Haag, F., Adriouch, S., Brass, A., Jung, C., Moller, S., Scheuplein, F., Bannas, P., Seman, M., Koch-Nolte, F., 2007. Extracellular NAD and ATP: partners in immune cell modulation. Purinergic Signal 3, 71–81.

Hu, X., Leak, R.K., Shi, Y., Suenaga, J., Gao, Y., Zheng, P., Chen, J., 2014. Microglial and macrophage polarization-new prospects for brain repair. Nat. Rev. Neurol.

Hwang, S.Y., Jung, J.S., Kim, T.H., Lim, S.J., Oh, E.S., Kim, J.Y., Ji, K.A., Joe, E.H., Cho, K.H., Han, I.O., 2006. Ionizing radiation induces astrocyte gliosis through microglia activation. Neurobiol. Dis. 21, 457–467.

Jeyaretna, D.S., Curry Jr., W.T., Batchelor, T.T., Stemmer-Rachamimov, A., Plotkin, S.R., 2011. Exacerbation of cerebral radiation necrosis by bevacizumab. J. Clin. Oncol. 29, e159–162.

Jiang, L.H., Mackenzie, A.B., North, R.A., Surprenant, A., 2000. Brilliant blue G selectively blocks ATP-gated rat P2X(7) receptors. Mol. Pharmacol. 58, 82–88.

Kaya, N., Tanaka, S., Koike, T., 2002. ATP selectively suppresses the synthesis of the inflammatory protein microglial response factor (MRF)-1 through Ca(2+) influx via P2X(7) receptors in cultured microglia. Brain Res. 952, 86–97.

Keystone, E.C., Wang, M.M., Layton, M., Hollis, S., McInnes, I.B., Team, D.C.S., 2012. Clinical evaluation of the efficacy of the P2X7 purinergic receptor antagonist AZD9056 on the signs and symptoms of rheumatoid arthritis in patients with active disease despite treatment with methotrexate or sulphasalazine. Ann. Rheum. Dis. 71, 1630–1635.

Kobayashi, K., Yamanaka, H., Noguchi, K., 2013. Expression of ATP receptors in the rat dorsal root ganglion and spinal cord. Anat. Sci. Int. 88, 10–16.

Lammer, A.B., Beck, A., Grummich, B., Forschler, A., Krugel, T., Kahn, T., Schneider, D., Illes, P., Franke, H., Krugel, U., 2011. The P2 receptor antagonist PPADS supports recovery from experimental stroke in vivo. PLoS One 6, e19983.

Lee, H.G., Won, S.M., Gwag, B.J., Lee, Y.B., 2011. Microglial P2X(7) receptor expression is accompanied by neuronal damage in the cerebral cortex of the APPswe/PS1dE9 mouse model of Alzheimer's disease. Exp. Mol. Med. 43, 7–14.

Lister, M.F., Sharkey, J., Sawatzky, D.A., Hodgkiss, J.P., Davidson, D.J., Rossi, A.G., Finlayson, K., 2007. The role of the purinergic P2X7 receptor in inflammation. J. Inflamm. (Lond.) 4, 5.

Liu, L., Duff, K., 2008. A technique for serial collection of cerebrospinal fluid from the cisterna magna in mouse. J. Vis. Exp.

Liu, S.F., Ye, X., Malik, A.B., 1999. Inhibition of NF-kappaB activation by pyrrolidine dithiocarbamate prevents In vivo expression of proinflammatory genes. Circulation 100, 1330–1337.

Liu, Y.P., Yang, C.S., Chen, M.C., Sun, S.H., Tzeng, S.F., 2010. Ca(2+)-dependent reduction of glutamate aspartate transporter GLAST expression in astrocytes by P2X(7) receptor-mediated phosphoinositide 3-kinase signaling. J. Neurochem. 113, 213–227.

Makoto, T., Hidetoshi, T.-S., Kazuhide, I., 2012. P2X4R and P2X7R in neuropathic pain. WIREs Membr. Transp. Signal. 1, 513–521.
Marcillo, A., Frydel, B., Bramlett, H.M., Dietrich, W.D., 2012. A reassessment of P2X7 receptor inhibition as a neuroprotective strategy in rat models of contusion injury. Exp. Neurol. 233, 687–692.
Matuschek, C., Bolke, E., Nawatny, J., Hoffmann, T.K., Peiper, M., Orth, K., Gerber, P.A., Rusnak, E., Lammering, G., Budach, W., 2011. Bevacizumab as a treatment option for radiation-induced cerebral necrosis. Strahlenther. Onkol. 187, 135–139.
Matute, C., Torre, I., Perez-Cerda, F., Perez-Samartin, A., Alberdi, E., Etxebarria, E., Arranz, A.M., Ravid, R., Rodriguez-Antiguedad, A., Sanchez-Gomez, M., Domercq, M., 2007. P2X(7) receptor blockade prevents ATP excitotoxicity in oligodendrocytes and ameliorates experimental autoimmune encephalomyelitis. J. Neurosci. 27, 9525–9533.
Monje, M.L., Toda, H., Palmer, T.D., 2003. Inflammatory blockade restores adult hippocampal neurogenesis. Science 302, 1760–1765.
Nandigam, R.N., Chen, Y.W., Gurol, M.E., Rosand, J., Greenberg, S.M., Smith, E.E., 2007. Validation of intracranial area as a surrogate measure of intracranial volume when using clinical MRI. J. Neuroimaging 17, 74–77.
Noone, T., 2006. An overview of steroid use and its potential side-effects. Nurs. Times 102, 24–27.
Olschowka, J.A., Kyrkanides, S., Harvey, B.K., O'Banion, M.K., Williams, J.P., Rubin, P., Hansen, J.T., 1997. ICAM-1 induction in the mouse CNS following irradiation. Brain Behav. Immun. 11, 273–285.
Panagiotakos, G., Alshamy, G., Chan, B., Abrams, R., Greenberg, E., Saxena, A., Bradbury, M., Edgar, M., Gutin, P., Tabar, V., 2007. Long-term impact of radiation on the stem cell and oligodendrocyte precursors in the brain. PLoS One 2, e588.
Peng, W., Cotrina, M.L., Han, X., Yu, H., Bekar, L., Blum, L., Takano, T., Tian, G.F., Goldman, S.A., Nedergaard, M., 2009. Systemic administration of an antagonist of the ATP-sensitive receptor P2X7 improves recovery after spinal cord injury. Proc. Natl. Acad. Sci. USA 106, 12489–12493.
Peng, Y., Lu, K., Li, Z., Zhao, Y., Wang, Y., Hu, B., Xu, P., Shi, X., Zhou, B., Pennington, M., Chandy, K.G., Tang, Y., 2014. Blockade of Kv1.3 channels ameliorates radiation-induced brain injury. Neuro Oncol. 16, 528–539.
Potucek, Y.D., Crain, J.M., Watters, J.J., 2006. Purinergic receptors modulate MAP kinases and transcription factors that control microglial inflammatory gene expression. Neurochem. Int. 49, 204–214.
Prinz, M., Priller, J., 2014. Microglia and brain macrophages in the molecular age: from origin to neuropsychiatric disease. Nat. Rev. Neurosci. 15, 300–312.
Routledge, J.A., Burns, M.P., Swindell, R., Khoo, V.S., West, C.M., Davidson, S.E., 2003. Evaluation of the LENT-SOMA scales for the prospective assessment of treatment morbidity in cervical carcinoma. Int. J. Radiat. Oncol. Biol. Phys. 56, 502–510.
Sharp, A.J., Polak, P.E., Simonini, V., Lin, S.X., Richardson, J.C., Bongarzone, E.R., Feinstein, D.L., 2008. P2x7 deficiency suppresses development of experimental autoimmune encephalomyelitis. J. Neuroinflammation 5, 33.
Skaper, S.D., Facci, L., Culbert, A.A., Evans, N.A., Chessell, I., Davis, J.B., Richardson, J.C., 2006. P2X(7) receptors on microglial cells mediate injury to cortical neurons in vitro. Glia 54, 234–242.
Sperlagh, B., Illes, P., 2014. P2X7 receptor: an emerging target in central nervous system diseases. Trends Pharmacol. Sci. 35, 537–547.
Stock, T.C., Bloom, B.J., Wei, N., Ishaq, S., Park, W., Wang, X., Gupta, P., Mebus, C.A., 2012. Efficacy and safety of CE-224,535, an antagonist of P2X7 receptor, in treatment of patients with rheumatoid arthritis inadequately controlled by methotrexate. J. Rheumatol. 39, 720–727.
Suzumura, A., Mezitis, S.G., Gonatas, N.K., Silberberg, D.H., 1987. MHC antigen expression on bulk isolated macrophage-microglia from newborn mouse brain: induction of Ia antigen expression by gamma-interferon. J. Neuroimmunol. 15, 263–278.
Tang, Y., Rong, X., Hu, W., Li, G., Yang, X., Yang, J., Xu, P., Luo, J., 2014. Effect of edaravone on radiation-induced brain necrosis in patients with nasopharyngeal carcinoma after radiotherapy: a randomized controlled trial. J. Neurooncol. 120, 441–447.
Wang, X., Arcuino, G., Takano, T., Lin, J., Peng, W.G., Wan, P., Li, P., Xu, Q., Liu, Q.S., Goldman, S.A., Nedergaard, M., 2004. P2X7 receptor inhibition improves recovery after spinal cord injury. Nat. Med. 10, 821–827.
Wang, Y.X., King, A.D., Zhou, H., Leung, S.F., Abrigo, J., Chan, Y.L., Hu, C.W., Yeung, D.K., Ahuja, A.T., 2010. Evolution of radiation-induced brain injury: MR imaging-based study. Radiology 254, 210–218.
Wang, Z., Yang, D., Zhang, X., Li, T., Li, J., Tang, Y., Le, W., 2011. Hypoxia-induced down-regulation of neprilysin by histone modification in mouse primary cortical and hippocampal neurons. PLoS One 6, e19229.
Yoritsune, E., Furuse, M., Kuwabara, H., Miyata, T., Nonoguchi, N., Kawabata, S., Hayasaki, H., Kuroiwa, T., Ono, K., Shibayama, Y., Miyatake, S., 2014. Inflammation as well as angiogenesis may participate in the pathophysiology of brain radiation necrosis. J. Radiat. Res. 55, 803–811.